Formation stages of bcc $(Fe_{44}Co_{44})Sn_{12}$ extended solid solution by mechanical alloying

J.M. Loureiro, B.F.O. Costa, B. Malaman, G. Le Caër, S. Das, V.S. Amaral

PII: S0925-8388(13)03050-8
DOI: http://dx.doi.org/10.1016/j.jallcom.2013.12.071
Reference: JALCOM 30135

To appear in:

Please cite this article as: J.M. Loureiro, B.F.O. Costa, B. Malaman, G. Le Caër, S. Das, V.S. Amaral, Formation stages of bcc $(Fe_{44}Co_{44})Sn_{12}$ extended solid solution by mechanical alloying, (2013), doi: http://dx.doi.org/10.1016/j.jallcom.2013.12.071

Formation stages of bcc $(Fe_{44}Co_{44})Sn_{12}$ extended solid solution by mechanical alloying

J.M. Loureiro[a], B.F.O. Costa[a], B. Malaman[b], G. Le Caër[c], S. Das[d], V.S. Amaral[d]

[a] CEMDRX, Physics Department, University of Coimbra, P-3004-516 Coimbra, Portugal

[b] Institut Jean Lamour, Département P2M, Equipe 103,CNRS(UMR7198)-Nancy Université, B.P.70239, F-54506 Vandoeuvre-les-Nancy Cedex, France

[c] IPR, UMR UR1-CNRS 6251, Université de Rennes I, Campus de Beaulieu, Bat 11A, F-35042 Rennes Cedex, France

[d] Department of Physics and CICECO, University of Aveiro, Campus de Santiago, P-3810-193 Aveiro, Portugal

Abstract:

The synthesis of supersaturated bcc $Fe_{44}Co_{44}Sn_{12}$ by mechanical alloying was followed by various techniques. Two stannides, $CoSn_5$ and $FeSn_2$ form first at interfaces. Tetragonal $CoSn_5$, a very recently discovered stannide, is obtained here by a simple method. These stannides then dissolve and the ternary bcc alloy forms with a progressive and simultaneous dissolution of Co and Sn into bcc Fe.

Keywords: Mechanical alloying, Fe-Co-Sn alloys, X-ray diffraction, Magnetization, Mössbauer spectroscopy

*Corresponding author:
Dr. B. F. O. Costa
Physics Department - University of Coimbra,
P-3004-516 Coimbra, Portugal
tel.: +351 239 410630
fax: +351 239 829158
email: benilde@ci.uc.pt

1- Introduction

Near-equiatomic FeCo alloys are b.c.c. below ~1250 K [1]. The b.c.c. phase (A2) orders to a CsCl type structure (B2) at temperatures below ~1000 K. Iron-cobalt alloys possess exceptional magnetic properties which make them useful as soft magnetic materials [1]. Various ternary or multinary systems based on near-equiatomic FeCo were thoroughly investigated [1]. The addition of a small amount of vanadium to FeCo helps for instance to circumvent its brittleness [1]. We started recently to study metastable $(Fe_{50-x/2}Co_{50-x/2})Sn_x$ ternary alloys prepared by mechanical alloying (MA) [2-3]. The structures and properties of alloys of the ternary system Fe-Co-Sn are essentially uninvestigated. The magnetic and magneto-optical properties of the compound FeCoSn, with a hexagonal Ni_2In type structure, were studied in ref. [4]. Ternary Fe-Co-Sn alloys were electrodeposited from a gluconate electrolyte [5]. Most of the alloys have a tin content larger than 82 at.%. The remaining alloys have compositions scattered around ~$Fe_{25}Co_{25}Sn_{50}$. An amorphous phase is the dominant phase in all these deposits. Co_2FeSn Heusler alloys films were prepared by controlled deposition of successive layers of Co, Fe and Sn [6]. In addition, Fe/MgO/Co_2FeSn magnetic tunnel junctions were characterized [6]. Finally, nanocrystalline tetragonal $(Fe_{1-y}Co_y)Sn_2$ were prepared by chemical methods to improve the electrochemical performance of Sn intermetallic compounds as electrode active material for Li-ion batteries [7].

Mechanical alloying was used successfully to enhance the solubility of Sn in bcc Fe from ~9 at% to ~20 at% [8-9]. The equilibrium solubility of Sn in FeCo (A2 or B2) is quite low at thermal equilibrium, being less than 1 at.% [10]. We chose thus MA as our preparation method to increase significantly the dissolution of tin in bcc

FeCo. A clear-cut value cannot be attributed readily to the actual supersaturation of as-milled $(Fe_{50-x/2}Co_{50-x/2})Sn_x$. In our milling conditions, the maximum solubility x_m, $14 \leq x_m \leq 20$, is likely closer to 20 [2-3]. The problems raised by the determination of x_m, which emphasize analogies between these ternary alloys and as-milled $Fe_{100-x}Sn_x$, will be discussed in detail elsewhere.

The phenomena which occur during MA from elemental powder mixtures were found to remain essentially unchanged for $(Fe_{50-x/2}Co_{50-x/2})Sn_x$ with $x \leq x_m$, being for instance qualitatively similar for x=6, 12 and 20. The present paper focuses on the mechanisms of mechanosynthesis of one of these alloys, namely $Fe_{44}Co_{44}Sn_{12}$. The milled powders were characterized as a function of milling time by a combination of various techniques: X-ray and neutron diffractions, magnetic measurements, Mössbauer spectroscopy of ^{57}Fe and ^{119}Sn.

2- Experimental

Powder mixtures of elemental Fe (purity: 99.9%), Co (purity: 99.8%) and Sn powders (purity: 99.5%) were mixed together and milled in argon atmosphere in a planetary Fritsch P6 ball-mill at 500 rpm for different milling times. The vials and the seven balls of 15 mm diameter used to mill were made of hardened steel. The powder to ball weight ratio was 1:20. X-ray diffraction (XRD) patterns were recorded using Cu $K\alpha$ radiation (λ = 0.1542 nm). SEM images and X-ray maps (Fe, Co, Sn) were obtained with a JEOL JSM 630 microscope. X-ray maps of particles of a powder milled for 12 h show that Fe, Co and Sn are homogeneously distributed. The latter sample is slightly enriched in Fe coming from milling tools, being actually $Fe_{46}Co_{42}Sn_{12}$. As this enrichment in Fe depends on milling time, the alloy will be denoted for convenience by its initial composition $Fe_{44}Co_{44}Sn_{12}$.

Magnetization measurements were carried out in a cryogen-free vibrating sample magnetometer (VSM) of CRYOGENIC Instruments with magnetic field up to 10 T and temperature in the range 1.7 K up to 320 K. The saturation magnetizations were measured at T=5 K. ^{57}Fe and ^{119}Sn Mössbauer spectra were recorded at room temperature (RT), in transmission geometry, by a constant acceleration type spectrometer using sources of ^{57}Co in Rh and of ^{119m}Sn in $CaSnO_3$ both with a strength of ~10 mCi. As usual, isomer shifts are referenced to α-Fe at RT and to SnO_2 for Fe and Sn respectively. Hyperfine magnetic field (HMF) distributions, P(B), were analyzed with a constrained Hesse-Rübartsch method [11] employing Lorentz lines. Here, P(B)ΔB represents the fraction of iron or tin atoms whose field lies between B and B+ΔB. The mean HMF's are denoted $<B_F>$ and $<B_S>$, where the indices F and S stand for ^{57}Fe and ^{119}Sn respectively. The 'width' of a distribution $P_X(B)$ (X=F,S) is characterized here by the standard-deviation $\sigma_X=<(B-<B_X>)^2>^{1/2}$.

3- Results and discussion

3.1 First stage: $0.5h \leq t_m \leq 2h$, stannide formation

In the MA process of ductile powder mixtures of A and B, particles are repeatedly flattened, fractured and welded. A layered structure of A and B is thus formed and progressively refined and convoluted ([12] and references therein). Interfaces thus play an important role in the synthesis process for short milling times. Three types of interfaces are formed in the case of Fe-Co-Sn: Co-Sn, Fe-Sn and Fe-Co. XRD patterns (fig.1) show broadened diffraction peaks of the starting elements, some of which become rapidly difficult to be evidenced. A broad line due to fcc Co is observed at ~52° for $t_m \geq 1h$ ('C' in fig.1). The other clearly visible peaks are associated with two

stannides: $CoSn_5$ and $FeSn_2$. During this first stage, fluctuations inherent to the as-prepared mixtures still persist but their magnitude weakens with t_m (ex: composition fluctuations from particle to particle). Therefore, the phenomena we describe below characterize the average behavior. Deviations from it may exist but they are often difficult to be evidenced and to be depicted with enough precision.

3.1.1 Co-Sn interfaces

The most intense lines at t_m=0.5h, indexed as '1' in fig.1 and other lines which are not seen at the scale of fig.1, are due to a compound "$CoSn_5$", possibly non-stoichiometric ($Co_{1-z}Sn_5$, z≈0.1-0.2), whose existence was unreported till recently [13]. Nanospheres of $CoSn_5$ were synthesized through a conversion chemistry route. It is tetragonal (*P4/mcc* space group) with lattice parameters are a=b=0.69328 nm, c=0.57924 nm [13]. The cobalt stannide formed by MA does not contain iron as confirmed by neutron diffraction patterns and by ^{119}Sn Mössbauer spectra recorded at 15K and at RT. Indeed, the ^{119}Sn spectra of $Co_{88}Sn_{12}$ milled for t_m=0.5h differ almost not from those of $Fe_{44}Co_{44}Sn_{12}$ (fig. 2). Therefore, $CoSn_5$ does not contribute to ^{57}Fe Mössbauer spectra. The intensities of $CoSn_5$ XRD peaks decrease rapidly. The main line is broad and weak at t_m=1.5h and is no more observed for t_m≥2h (fig. 1). We found that $CoSn_5$ forms too in the early stage of MA of Co-Sn alloys at any Sn content ranging between 6 and 83 at.%. The very rapid formation of $CoSn_5$ at Co-Sn interfaces can be understood from the fact that Co is an anomalously fast diffuser into Sn [14]. $CoSn_5$ is non-magnetic as are all tin-rich cobalt stannides.

3.1.2 Fe-Sn interfaces

The second stannide ('2' in fig.1) is tetragonal $FeSn_2$ with a $CuAl_2$ type structure (*I4/mcm* space group) and a=b=0.6539 nm, c=0.5325 nm. The most intense XRD peak of $FeSn_2$ is still seen at t_m=3h. Its decrease starts at t_m~2h. This distannide may become enriched in Co when MA proceeds. The XRD line positions, which remain essentially unchanged with t_m, indicate however that Co remains a minor alloying element (fig.1 of [7]). $FeSn_2$ is repeatedly reported to form at Fe-Sn interfaces in all kinds of experiments and notably during the mechanosynthesis of Fe-Sn alloys [8-9]. The clear asymmetry of the central part of the ^{57}Fe Mössbauer spectra observed for $t_m \leq 2$h (fig. 2) is consistent with the formation of antiferromagnetic $FeSn_2$ [15] which becomes superparamagnetic when nanostructured. Its ^{57}Fe spectrum consists then in a single line at 0.50 mm/s [7,15]. $FeSn_2$ forms more slowly than $CoSn_5$.

3.1.3 Fe-Co interfaces

For short milling times, Fe-Co interfaces favor the formation of solid solutions whose compositions fluctuate. The lattice parameter of the bcc phase ('F' in fig. 1) remains essentially constant for $t_m \leq 2$h (fig. 3). This result can only be explained by the formation or Fe-rich bcc Fe-Co alloys, with a Co content less than ~25 at.%, a concentration range in which the lattice parameter of bcc Fe-Co alloys varies very little [16]. These Fe-Co alloys remain thus unobserved in ^{119}Sn Mössbauer spectra. Simultaneously, the ^{57}Fe Mössbauer spectra evolve slightly (fig. 2). The associated HMF distributions $P_F(B)$ go through a maximum for the field of bcc α-Fe at RT, 33.1T (fig.4). Most of the central part of $P_F(B)$ is indeed due to unalloyed bcc Fe. The amplitude of $P_F(B)$ and the mean-field $\langle B_F \rangle$ decrease (table 1). Simultaneously, the standard deviation increases because of the progressive growing of both low-field and

high-field tails (fig.4). From the concentration dependence of the mean ^{57}Fe HMF in Fe-Co alloys [16], the low-field tail is attributed to hcp or fcc Co-rich Co-Fe alloys, with a Co content larger than ~80 at.%, while the high-field tail is ascribed to bcc Fe-rich Fe-Co alloys with a Co content less than ~25 at.% in agreement with XRD.

The decrease of the saturation magnetization for $t_m \leq 2h$ (fig. 3) is primarily due to the formation of the previous stannides. ^{119}Sn Mössbauer spectra for t_m=1.5h and 2h shows the presence of a magnetic component (fig.2). Some HMF distributions are plotted in fig.4 for ^{119}Sn and ^{57}Fe. Once $CoSn_5$ begins to disappear, tin is released and starts to dissolve locally into hcp and fcc cobalt. A similar phenomenon occurs later with $FeSn_2$ and bcc Fe. The HMF's of ^{119}Sn dissolved in bcc Fe, hcp Co and fcc Co at RT are respectively 7.9T [17], 4T [18] and 1.7T [18]. The HMF distribution of fig.4 (t_m=1.5h) is consistent with the transient formation of Fe and Co alloys with limited contents of Sn. The evaluation of the relative amounts of Sn engaged in the various phases from Mössbauer spectra must be cautious as long as β-Sn has not disappeared because the latter phase has a very small Lamb-Mössbauer factor at RT (~0.04, [19]). Further, its disappearance is better judged from Mössbauer spectra than from XRD because of nanometer-sized grains. In any case, no significant amounts of concentrated bcc Fe-Sn or Fe-Co-Sn can be formed during this first step because the lattice parameter would otherwise increase [2-3, 17] in contradiction with experiment.

3.2 Second stage: $t_m \geq 2.5h$

For $t_m > 2h$, the lattice parameter "a" of the bcc phase and the saturation magnetization increase and reach a plateau at $t_m > \sim 8h$ (fig.3). Similarly, the ^{57}Fe Mössbauer lines broaden progressively, $\langle B_F \rangle$ decreases and σ_F increases (fig.2, table 1). $\langle B_S \rangle$ increases first and then it levels off at a field of 10T for $t_m \geq 8h$ (table 1), a

value discussed in detail in [2-3]. These results imply the formation of a bcc ternary alloy progressively enriched in Sn. This tin enrichment must be fast enough as compared to the speed of dissolution of cobalt into the bcc phase to prevent i) a decrease of "a", which occurs for Co contents larger than ~28 at.% in bcc Fe-Co alloys [16], ii) an overshoot of the average magnetic moment per transition metal atom $<\mu>$ and iii) an ensuing increase of $<B_F>$ (36T for ~30 at.% Co [16]). Indeed, $<\mu(0)>=(\mu_{Fe}+\mu_{Co})/2=1.97\mu_B$/at(Fe,Co) for as-prepared $Fe_{44}Co_{44}Sn_{12}$ powder mixtures while the final moment of our ternary alloy is $2.01\mu_B$/at(Fe,Co) (fig.3). Both are smaller than $<\mu>$ for bcc Fe-Co with ~30 at.% Co, $2.46\mu_B$/at(Fe,Co). The moment $<\mu(t_m)>$ increases during the second stage on the one hand because of the progressive dissolution of the stannides formed during the first stage and on the other because of the formation of a ternary bcc alloy whose composition evolves progressively to the final one. When the tin HMF's in bcc Fe-Co-Sn alloys increase on average, then the inner lines of the associated magnetic subspectra move apart and a central peak becomes visible ($t_m \geq 3.5$h, fig. 2). Its intensity goes through a maximum and then decreases almost to zero. Simultaneously, a low intensity and broad XRD peak appears at ~30° for $2.5\text{h} \leq t_m \leq 6\text{h}$ (fig.1 and inset for t_m=4h).

The halo at ~30° might be due to an amorphous tin oxide. The XRD pattern (Cu Kα) of amorphous SnO has its main component centered at 30° [20] while the first broad peak of amorphous SnO_2 is found at ~26° [21]. An amorphous SnO_z oxide, with $1<z<2$, would be needed to explain the central ^{119}Sn peak (fig. 2). The first halo of such an oxide is expected however to shift to angles smaller than 30°. The halo at ~30° might come from another amorphous phase. Indeed, the Cu Kα XRD patterns reported for amorphous $Co_{100-x}Sn_x$ alloys prepared by different methods (sputtering, $26 \leq x \leq 45$ [22], solvothemal route, x=40 [23], MA, x=15, 35, 50 [24]) are all similar

with a broad first halo at ~31°. A similar peak is observed on the XRD pattern of MA $Fe_{75}Sn_{25}$ (fig.5 of [9]). A second halo is seen at ~43° [22] and would be hidden here by the main bcc peak. The halo positions observed on CoKα XRD patterns of amorphous Fe-Co-Sn [5], once converted to CuKα radiation, are in full agreement with the previous value. Thus, the small peak (inset of fig.1) might be too attributed to an amorphous Co-Fe-Sn alloy but the transient central ^{119}Sn peak would still remain to be explained. At this point, it is difficult to decide which of the two attributions of the small intensity XRD peak is to be retained. Further, both might coexist. Additional characterization is needed to solve this question. Finally, the supersaturated bcc phase in dynamical equilibrium in our milling conditions is found for $t_m \geq 8h$.

4- Conclusion

The mechanical alloying of supersaturated bcc $Fe_{44}Co_{44}Sn_{12}$ was studied as a function of milling time. Two stannides, $CoSn_5$ and $FeSn_2$, form first at interfaces. Tetragonal $CoSn_5$, a very recently discovered stannide [13], is obtained here by a simple method. Its very rapid formation results from the anomalously fast diffusion of Co into Sn. These stannides dissolve and the ternary bcc alloy form with a simultaneous dissolution of Co and Sn into bcc Fe until the dynamic equilibrium phase is obtained. The MA mechanisms are qualitatively similar for all supersaturated bcc alloys we studied (Sn content: $x \leq 20$). The as-milled alloys ($x \leq 20$) order by annealing during 15h at 673K as proven unambiguously by neutron diffraction patterns and ^{119}Sn Mössbauer spectra (in preparation).

Acknowledgements

The financial support of the bilateral Portuguese-French program FCT-CNRS, that of J.M. Loureiro (FCT, Grant SFRH/BD/44130/2008) and the FCT/COMPETE PEst-C/FIS/UI0036/2011 project are gratefully acknowledged.

References

[1] T. Sourmail, Progr. Mater. Sci. **50** (2005) 816-880.

[2] J.M. Loureiro, B.F.O. Costa , G. Le Caër, J. Alloy Compd. **536S** (2012) S31-S34.

[3] J.M. Loureiro, B.F.O. Costa, G. Le Caër , B. Malaman, Solid State Phenom. **194** (2013) 187-193.

[4] K.H.J. Buschow and P.G. van Engen, Phys. Stat. Sol. (a) **76** (1983) 615-620.

[5] C. Chisholm et al., Appl. Surf. Sci. **253** (2007) 4348–4355.

[6] M. A. Tanaka et al., J. Appl. Phys. **111** (2012) 053902 (4 pp).

[7] U. G. Nwokekea, A. V. Chadwick, R. Alcantara, M. Alfredsson and J. L. Tirado, J. Alloy Compd. **509** (2011) 3074–3079.

[8] A. F. Cabrera, F. H. Sánchez and L. A. Mendoza Zélis, Phys. Rev. B **53** (1996) 8378-8385.

[9] G. A. Dorofeev and E. P. Elsukov, Inorg. Mater. **36** (2000) 1228-1234.

[10] N.N. Delyagin and E.N. Kornienko, Sov. Phys. Sol. St., **13**, 1254 (1971).

[11] G. Le Caër and J. M. Dubois, J. Phys. E **12** (1979)1083–1090.

[12] E. Gaffet et al., J. Mater. Chem. **9** (1999) 305–314.

[13] X.L. Wang, H. Chen, J. Bai and W.Q. Han, J. Phys. Chem. Lett. **3** (2012) 1488−1492.

[14] P. Guilmin, P. Guyot and G. Marchal, Phys. Lett. **109A** (1985) 174-178.

[15] M. Chamas, M.T. Sougrati, C. Reibel and P.E. Lippens, Chem. Mater. **25** (2013) 2410−2420.

[16] E Jartych, J K Zurawicz and M Budzynski, J. Phys.: Condens. Matter **5** (1993) 927-934.

[17] E.P. Yelsukov et al., J. Magn. Magn. Mater. **166** (1997) 334-348.

[18] M. Semba, P. Raghavan, W. Semmler and R.S. Raghavan, Hyperfine Interact. **9** (1981) 449-452.

[19] C. Hohenemser, Phys. Rev. **139** (1965) A185-A196.

[20] K.M. Lee, D.J. Lee and H. Ahn, Mater. Lett. **58** (2004) 3122-3125.

[21] Y. Caglar, S. Ilican and M. Caglar, Eur. Phys. J. B **58** (2007) 251-256.

[22] A.D.W. Todd, R.A. Dunlap and J.R. Dahn, J. Alloy Compd. **443** (2007) 114–120.

[23] J. Xie, X.B. Zhao, G.S. Cao and J.P. Tu, J. Power Sources **164** (2007) 386–389.

[24] V.M. Lopez Hirata, F. Martinez Suarez and J.G. Cabanas Moreno, Mater. Sci. Eng. A **181-182** (1994) 1258-1262.

Table 1: Mean ^{119}Sn (S) and ^{57}Fe (F) HMF's and standard-deviations at different milling times ($<B_S>$=0T and $<B_F>$=33.1T at t_m=0)

t_m(h)	$<B_S>$ (T)	σ_S (T)	t_m(h)	$<B_F>$ (T)	σ_F (T)
1.5	6.9 ± 0.2	3.4 ± 0.2	0.5	32.9 ± 0.2	1.7 ± 0.2
2	8.2 ± 0.3	4.7 ± 0.3	2	32.4 ± 0.3	2.4 ± 0.3
≥ 8	10.1 ± 0.3	4.5 ± 0.3	12	31.2 ± 0.2	3.3 ± 0.3

Figure Captions

Figure 1- Evolution with milling time, t_m (h) (indicated on the left), of the X-ray diffraction patterns (Cu$K\alpha$) of mechanically alloyed $Fe_{44}Co_{44}Sn_{12}$.

Figure 2- Room-temperature ^{119}Sn (left) and ^{57}Fe (right) Mössbauer spectra of mechanically alloyed $Fe_{44}Co_{44}Sn_{12}$ as a function of milling time t_m (h) (indicated on the left).

Figure 3- Evolution with milling time, t_m (h), of two characteristics of mechanically alloyed $Fe_{44}Co_{44}Sn_{12}$: left) lattice parameter of the bcc phase evidenced in X-ray diffraction patterns (fig. 1) right) saturation magnetization at 5K.

Figure 4- Hyperfine magnetic field distributions at RT of $Fe_{44}Co_{44}Sn_{12}$ for the indicated milling times: ^{119}Sn (left) and ^{57}Fe (right).

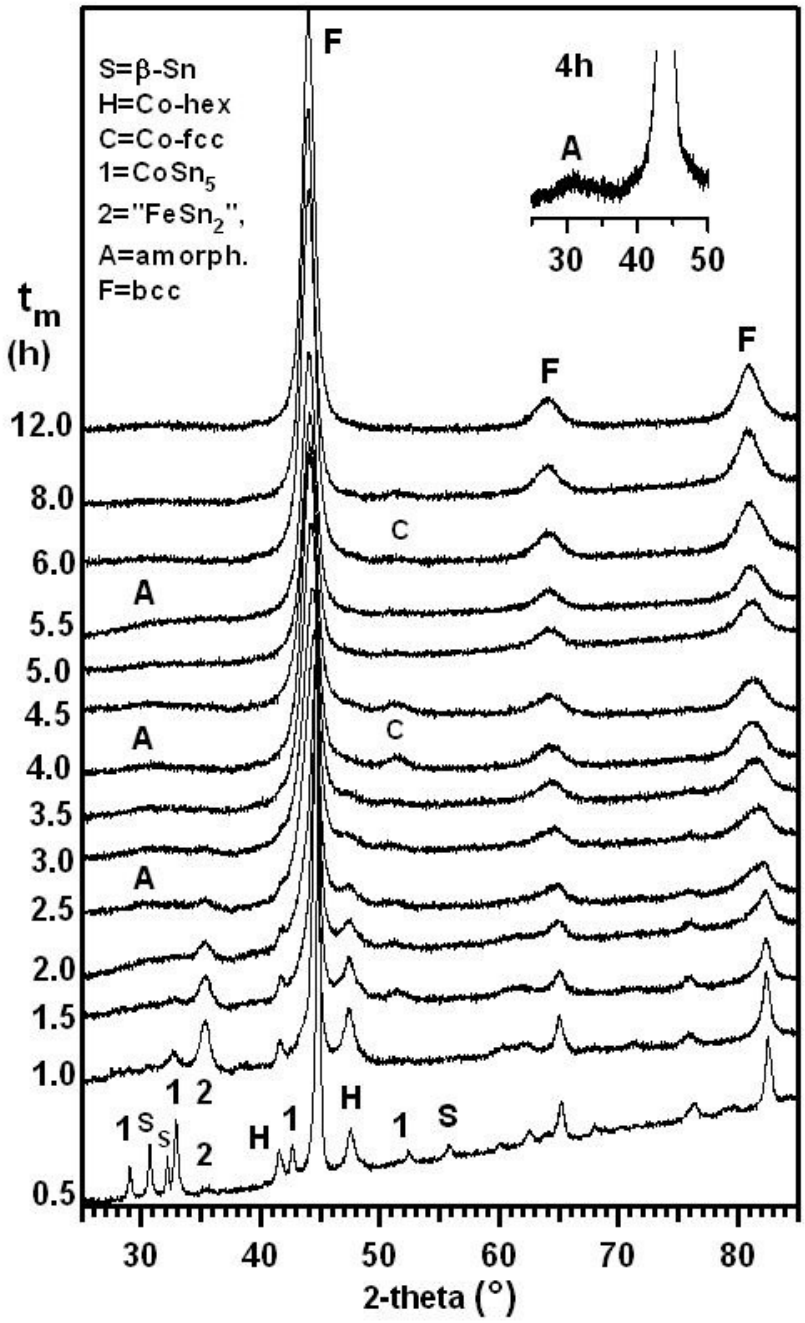

Figure 1- Evolution with milling time, t_m (h) (indicated on the left), of the X-ray diffraction patterns (Cu$K\alpha$) of mechanically alloyed $Fe_{44}Co_{44}Sn_{12}$.

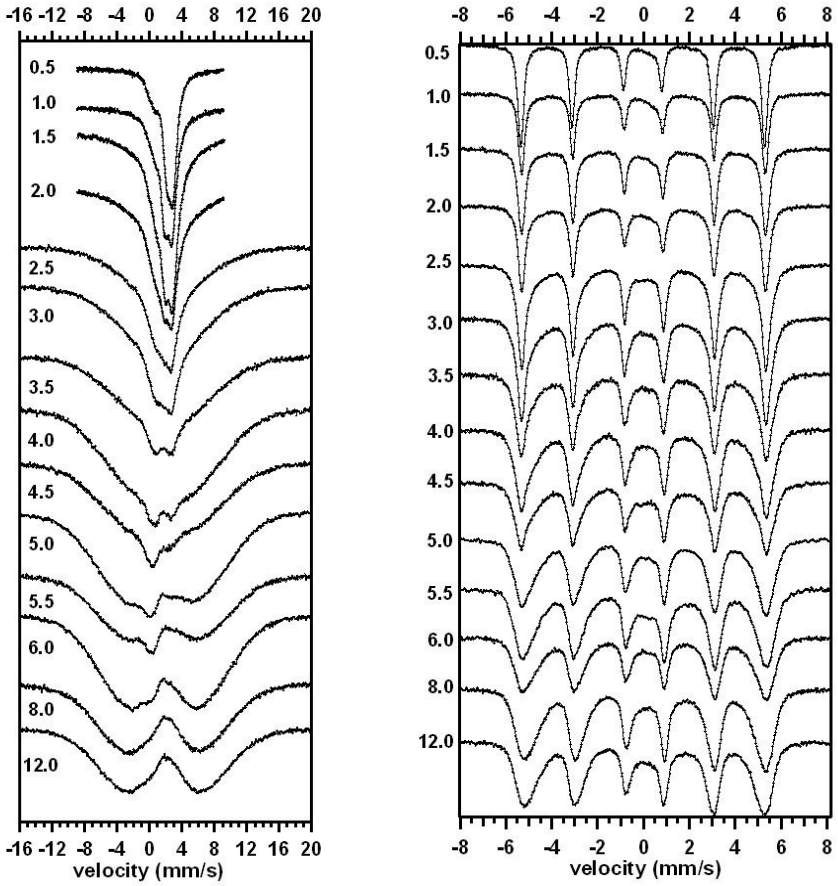

Figure 2- RT ^{119}Sn (left) and ^{57}Fe (right) Mössbauer spectra of mechanically alloyed $Fe_{44}Co_{44}Sn_{12}$ as a function of milling time t_m (h) (indicated on the left).

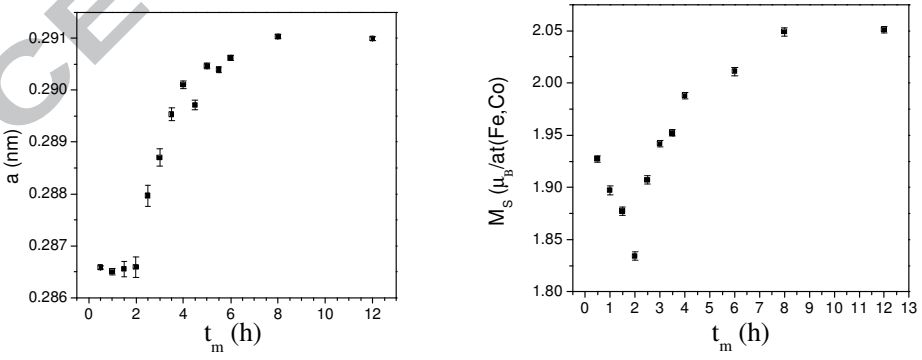

Figure 3- Evolution with milling time, t_m (h), of two characteristics of mechanically alloyed $Fe_{44}Co_{44}Sn_{12}$: left) lattice parameter of the bcc phase evidenced in X-ray diffraction patterns (fig. 1), right) saturation magnetization at 5K.

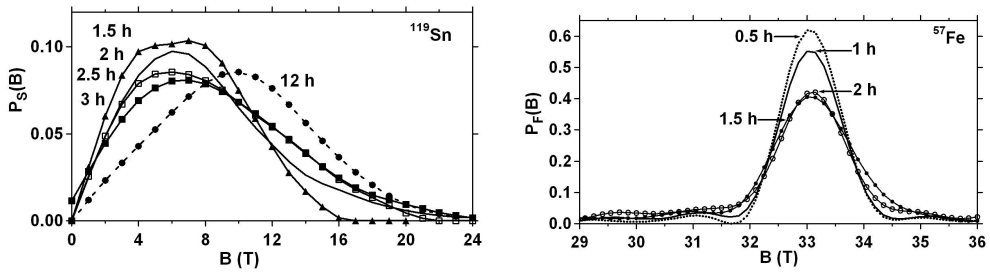

Figure 4- Hyperfine magnetic field distributions at RT of $Fe_{44}Co_{44}Sn_{12}$ for the indicated milling times: ^{119}Sn (left) and ^{57}Fe (right).